iJRASET
International Journal For Research in Applied Science and Engineering Technology

INTERNATIONAL JOURNAL FOR RESEARCH

IN APPLIED SCIENCE & ENGINEERING TECHNOLOGY

Volume: 9 **Issue:** VII **Month of publication:** July 2021

DOI: https://doi.org/10.22214/ijraset.2021.37124

www.ijraset.com

Call: 08813907089 | E-mail ID: ijraset@gmail.com

International Journal for Research in Applied Science & Engineering Technology (IJRASET)
ISSN: 2321-9653; IC Value: 45.98; SJ Impact Factor: 7.429
Volume 9 Issue VII July 2021- Available at www.ijraset.com

Single Stage Autonomous Solar Water Pumping System Using PI and Fuzzy Controllers

Bujula Harikrishnareddy
JNTUA, India

Abstract: ***Sustainable powerage and viable use of accessible energy assets have arisen as an commendable panacea for expanding carbon impression, draining petroleum derivatives, expanding a dangerous atmospheric deviation and changing meteorological situations. Flawless nature, silent activity and bountiful accessibility even at distant areas, have made the sunlight based energy finest form of RE accessible in the current situation .The work presents a introverted stage independent sun oriented photovoltaic exhibit take care of water siphoning framework utilizing a long-lasting magnet simultaneous engine. The crucial commitment of this work incorporates advancement of novel altered vector control, which improves the force reaction of the framework and improvement of a novel single stage variable advance size gradual conductance strategy, which gives a quick greatest force point following and dispenses with the need of transitional stage DC-DC converter. A corresponding indispensable control diminishes the mistake among reference and real value. The utilization of single stage geography has killed middle stage DC-DC converter and diminished the quantity of components, consequently bringing about decrease of the expense, intricacy and increment efficiency .The expansion of this activities rather than PI regulators that we need to Fuzzy and PI regulators .Utilizing this controllers step reaction of speed increases, Dc-connect voltage increases and force speed proportion is all the more then, at that point power stream will be improved. The framework execution has been examined through Matlab /simulink recreation investigation***

Keywords: Solar water pumping, maximum power point tracking, maximum power point algorithm, PMSM drive, fuzzy and PI controllers.

I. INTRODUCTION

Manageable power age and suitable utilization of open energy resources have emerged as an honorable panacea for growing carbon impression, depleting petrol subsidiaries, extending a risky air deviation and changing meteorological circumstances. Immaculate nature, quiet action and plentiful ingenuousness even at far off regions, have made the sunshine based energy best type of RE available in the current circumstance. Diminishing capital expense, negligible conservation cost and zero working expense, have made sun oriented photovoltaic (SPV) framework a brilliant possible approach to outfit sun oriented energy [3-4]. As of late, SPV take care of water siphoning is getting more extensive consideration [5]. For regions having no ingenuousness to the framework and great sun oriented insolation accessibility for a large portion of days in a year, the sunlight based water siphoning (SWP) is meeting the water prerequisite for every day fundamental exercises [6]. Also, SWP is giving an incredible lift to agrarian and modern exercises [7-8].SPV coordinated water siphons experience a portion of the potential difficulties like diminished effectiveness, expanded DC interface voltage shakiness, lazy reaction and high capital expense [9]. In spite of the fact that a few explores have been completed to relieve a portion of these challenges, in any case lacking writing is accessible to adapt up with this load of issues. This work is expected to meet the vast majority of the issues related with SWP. Ordinary drives utilized for SWP are very profligate. The development of permanent magnet drives has prompted decrease in misfortunes up indeed. Permanent magnet synchronous machines (PMSM) and brushless DC machines (BLDC) are the two generally utilized variation of lasting magnet machines [10]. PMSM have instinctive benefits of high proficiency, low force swells, low clamor, high air hole motion thickness, high ability to weight proportion, high force to latency proportion, fast speed increase and deceleration ability, high force factor furthermore, minimized plan [11]. This makes the engine most appropriate for SWP. A large portion of the current geographies for SWP, use acceptance engine (IM) for driving the siphon, be that as it may, a relative field test examination performed by Brinner et.al. [12] on electric sub siphon (ESP) uncovers that the permanent magnet machines (PMM) based ESP offers 20 % decreased utilization contrasted with IM based ESP of comparable rating.

As the open loop control of PMSM, isn't suggested, PMSM endures the downside of complex speed control. Vector or field arranged control and direct force control (DTC) are by large utilized methods for speed control of PMSM [13]. DTC is more straight forward when contrasted with vector control, however, it's anything but an inherent issue of expanded force and transition swells. This issue has been tended to in different existing writing, be that as it may, the arrangement comes either at the expense of expanded computational weight or expanded equipment parts [14-15].

ISSN: 2321-9653; IC Value: 45.98; SJ Impact Factor: 7.429
Volume 9 Issue VII July 2021- Available at www.ijraset.com

V/f is likewise one of the once in a while utilized method for speed control of PMSM as it's anything but a downside of snoozing reaction and requires balancing out circles for high velocity activity [16-17]. Vector control procedure gives an astonishing pace control [18]. Here execution ability, PMSM is changed over to identical independently energized DC machine [19].

The DC machine enjoys a benefit of decoupled symmetrical transition and force parts. The transition and force are controlled, individually by controlling field current (I_f) and armature current (I_a). This control is stretched out to PMSM by thinking about the engine in a simultaneously rotating reference outline (d-q) so that the sinusoidal amounts look like DC in consistent state condition. The symmetrical direct (d) hub and quadrature (q) axis flows are the parts of stator current and can be controlled independently comparable to a DC machine. The reference direct pivot current is controlled as per required transition, though the reference quadrature pivot current is controlled as per the required force. A changed vector control (MVC) strategy is utilized here, through using an additional control circle for example force control circle and a SPV power feed-forward term (FFT). The joining of force control circle diminishes the weight on the speed regulator and further develops the force reaction while the presentation of SPVFFT speeds up the general reaction of the framework. For the extraction of ideal force from SPV cluster, greatest force point following (MPPT) strategies are utilized. Various MPPT procedures like a gradual conductance (INC), annoy and notice (P&O), fluffy rationale control, neural network, partial Voc, fragmentary Isc and numerous other are talked about in the current writing. Podder et al. [20] have introduced an indepth examination of various MPPT procedures.

MPPT strategies, P&O and INC are the two generally utilized strategies for SWP [21-23]. The P&O shows a straight forward control approach including bother of the SPV cluster voltage towards the most extreme force point (MPP). Be that as it may, this strategy experiences the downside of consistent state motions due to annoyances [21]. These motions bring about power misfortune and are ineffectual for most extreme force extraction. The rule in question in MPPT utilizing an INC technique, depends on the way that the steady conductance and momentary conductance of the SPV cluster are equivalent at MPP [22]. Hypothetically, this strategy gives no consistent state motions as once the MPP is reached, there is no need of any further annoyance until the adjustment of conductance happens. Notwithstanding, because of the viable restriction of goal of step size, the motions are non-zero constantly [23]. Indeed despite the fact that P&O method is straightforward and effectively implementable, an INC calculation gives exact and quick MPP following during drifters. An INC strategy for MPPT ordinarily has fixed advance size by and by, Yang et al. [24] have proposed an INC calculation that utilizes variable advance size by adjusting the progression size of the obligation proportion with each emphasis. In any case, as proposed calculation can be utilized just for two phase MPPT, it is notable that a solitary stage geography wipes out the necessity of transitional DC-DC converter and, thusly, better from the view point of proficiency, size and cost. Keeping the advantages of single stage geography in see, this work utilizes a solitary stage variable advance size gradual conductance (VSS-INC) MPPT calculation. This framework for SWP is planned, demonstrated and mimicked under MATLAB/Simulink climate and the equipment approval is completed on a created model in the research facility. This framework utilizes a solitary stage VSS-INC MPPT calculation for ideal force extraction from SPV cluster and MVC for speed control of PMSM. The setup for SWP frame work, is displayed in Fig. 1. This framework contains (from left to right) SPV exhibit, a three-stage voltage source inverter (VSI), a PMSM and a water siphon. A diode (D) is utilized between SPV exhibit and VSI to stop the progression of any switch current into SPV cluster. The SPV exhibit comprises of fitting number of series and equal blend of SPV modules. As the photons strike the outside of the SPV cluster, electrical energy is produced. This produced electrical energy is taken care of to the DC connection of VSI. The VSI goes about as force preparing unit. It pivots the PMSM with pump coupled to it and in this way changes over this electrical energy into rotational mechanical energy. This SWP framework comprises of just a single energy putting away component for example DC interface capacitor (C_{dc}). Expecting the framework to be lossless, during transient condition

$$P_{pv} = P_{C_{dc}} + P_m \quad (1)$$

$$P_{C_{dc}} = V_{dc} C_{dc} \frac{dV_{dc}}{dt} \quad (2)$$

Where, P_{pv}, P_{Cdc} and P_m are PV array, DC link capacitor and motor output power, respectively.

$$P_{pv} = V_{dc} C_{dc} \frac{dV_{dc}}{dt} + \tau_m \omega_m \quad (3)$$

Where, τ_m and ω_m are motor torque and speed, respectively.
During steady state condition, V_{dc} remains constant.

Therefore, $\frac{dV_{dc}}{dt} = 0$ (4)

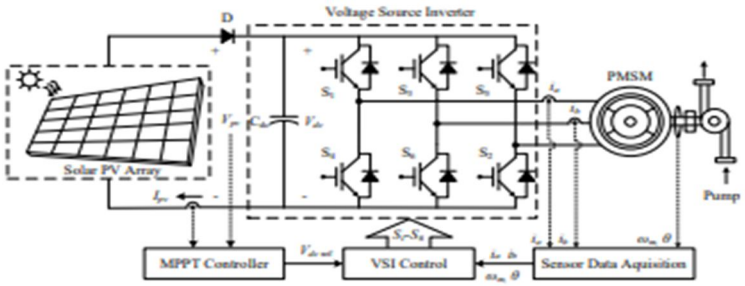

Fig. 1 Configuration diagram of SWP system

Hence, (3) becomes as,

$$P_{pv} = 0 + \tau_m \omega_m \quad (5)$$

For a pump type load, the torque is considered as,

$$\tau_m \propto \omega_m^2 \quad (6)$$

Let K_m be pump proportional constant.

Since $\tau_m = K_m \omega_m^2$ (7)

Therefore, (5) becomes,

$$P_{pv} = K_m \omega_m^3 \quad (8)$$

The connection (8) uncovers that the SPV cluster power (P_{pv}) is corresponding to the 3D shape of engine speed (ω_m). This epitomizes that for appropriate MPPT following, the reference engine speed (ω_{ref}) must be gotten appropriately. For this framework, ω_{ref} includes two sections; $\omega_{ref\,1}$ and $\omega_{ref\,1}$ and $\omega_{ref\,2}$ as displayed in Fig. 2 (b). ω_{ref1} comes from DC connect voltage regulator. VSS-INC calculation utilizes the SPV cluster voltage (V_{pv}) and current (I_{pv}) as information sources and these create a reference DC connect voltage ($V_{dc\,ref}$) needed for the activity at MPP. For single stage geography, the DC connect voltage (V_{dc}) is same as V_{pv} consequently they can be utilized reciprocally. $V_{dc\,ref}$ is contrasted and $_{Vdc}$ and the mistake is taken care of to DC connect voltage regulator, which diminishes the DC interface voltage error to zero by changing $\omega_{ref\,1}$ and $\omega_{ref\,2}$ comes from FFT, which is an element of SPV power (P_{pv}). Since $\omega_{ref\,2}$ is a direct capacity of P_{pv} and includes no regulator in the middle, any change in P_{pv} straight forwardly prompts change in $\omega_{ref\,2}$ which makes the framework reaction quicker. After the age of ω_{ref}, the speed of PMSM is controlled utilizing MVC. For this ω_{ref} is contrasted and ω_m and the speed mistake (ω_{error}) is taken care of to the speed regulator. The yield of the speed regulator is considered as reference electromagnetic force (Te_{ref}).

The Te_{ref} is contrasted and assessed electromagnetic force (Te_{est}) and the torque error (Te_{error}) is produced. The Te_{error} is taken care of to the torque regulator and the yield is considered as reference quadrature axis current (level of intelligence ref), which is further used for speed control of PMSM. The age of intelligence level ref utilizing ordinary and MVC is displayed in Fig. 2 (a), and Fig. 2 (b), individually. An explained conversation of VSS-INC and MVC, is introduced in area IV (a) and IV (b), separately.

(a)

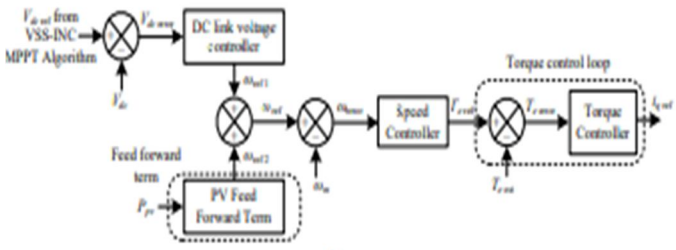

(b)

Fig. 2 $i_{q\,ref}$ generation using (a) Conventional and (b) Modified vector control

II. SYSTEM DESIGN

For the development of an effective SWP system and to make it capable to perform under different operating conditions, various sections shown in Fig. 1, need to be designed appropriately. A PMSM of a power rating of 7.8 kW is selected to design this system. An elaborated design of SPV array and DC link capacitor are as follows.

A. Design of SPV array

Sunlight based cells are utilized for changing over the energy of photons into electrical energy. A technique for the displaying of sunlight based cell, has been introduced by Venkatramanan et.al. [25]. Same technique is utilized here for the displaying of SPV exhibit.

The power rating of the SPV exhibit incredibly relies upon the force rating of the load. To make up for the misfortunes caused in the transitional stages between SPV cluster and the load, predominately the power rating of the SPV exhibit is taken nearly nothing higher to that of the load. For the agreeable activity of a PMSM of 7.8 kW, a SPV exhibit having a pinnacle capacity of 8.4 kW under standard test condition (STC, STC: 1000 W/m² , 25 °C) is planned. The SPV exhibit comprises of low force rating SPV modules, which are collected in series and equal depending upon required voltage and current rating, separately. A name sun based PV module KC200GT fabricated by Kyocera is considered for the plan of SPV cluster [26]. The necessary SPV exhibit power, Ppv = Pmpp = 8.4 kW (9) Where, Pmpp is the SPV cluster power at MPP. Quantities of required SPV modules, are given as,

$$n = \frac{P_{mppp}}{P_{mp}} = \frac{8400}{200.143} \approx 42$$

For a single stage topology, SPV array MPP voltage Vmpp is chosen near about to the DC link voltage (V_{dc}). The V_{dc} for the PMSM model selected in this work is 560 V. Numbers of SPV modules connected in series are given as,

$$n_s = \frac{V_{mppp}}{V_{mp}} = \frac{560}{26.3} \approx 21 \text{ modules}$$

Numbers of SPV modules connected in parallel are given as,

$$n_p = \frac{P_{mppp}}{n_s * V_{mp} * I_{mp}} = \frac{8400}{21*26.3*7.61} \approx 2 \text{ modules}$$

The SPV array constitutes a total of 42 SPV modules arranged in 2 parallel paths of 21 modules connected in series in each path.

B. Design of a DC Link Capacitor

The value of DC link capacitor can be evaluated as

$$C_{dc} = \frac{I_0}{2*\omega_e*\Delta V_{dc}} = \frac{8400/560}{2*314.16*0.02*560} = 2132\mu F$$

Where, Io = P_{mpp}/V_{dc}, ΔV_{dc} is % ripple voltage taken as 2% of V_{dc} and ω_e = 2*π*50 =314.16 rad/s is the angular frequency. The calculated value of DC link capacitor is 2132 µF. A standard value of capacitor available is 2200 µF, so the C_{dc} = 2200 µF.

C. System Control Strategy

The control of this system shown in Fig. 1, is divided into two parts. First part is devoted for maximum power extraction from SPV array using single stage VSS-INC algorithm, whereas, the second part is dedicated for the speed control of PMSM using MVC. A proportional integral (PI) controller reduces the error between reference and actual value. This configuration utilizes three PI controllers. First PI controller ensures the MPP operation by reducing the DC link voltage error while the second and third PI controllers are used for MVC. The second PI controller reduces the speed error and third PI controller reduces the torque error. A SPV-FFT is incorporated to accelerate the system transient response.

D. Single Stage Variable step size Incremental Conductance (VSS-INC) Technique

The progression size of the VSS- INC technique is generally fixed. The more advance size brings about slow unique execution and more consistent state motions while the bigger advance size results in quick unique execution and expanded consistent state motions. Both the circumstances lead to wastage of force as an normal yield power is fundamentally diminished. This issue can be settled by keeping the progression size variable with the end goal that during transient, the progression size would be huge guaranteeing quick elements and during consistent express the progression size would be little guaranteeing altogether diminished motions. The calculation for VSS-INC, is displayed in Fig. 3. This calculation gives Vdc ref as a yield required for single stage MPPT. The generation of vdc reference is taken as

$$V_{dc\,ref}(k) = V_{dc\,ref}(k-1) \pm Step$$

The value of step is variable and is calculated as,

$$Step = K_{vs} * \left| dP_{pv} / dV_{pv} \right|$$

Where, Kvs is the step size constant, dPpv and dVpv are the difference in SPV array power and SPV array voltage at kth and (k-1) th sampling instant, respectively.

The other equations involved in VSS-INC algorithm are shown in Fig. 3. The selection of Kvs greatly affects the MPPT performance. The determination of k_{vs} is based on the fact that a larger step size Stepmax is initially opted for fast dynamic response during starting.

During beginning the consistent state value rather than dynamic value of the |dPpv/dVpv| is determined under the consistent step size activity with Stepmax, which is the maximum furthest reaches of the VSS-INC. It is seen that |dPpv/dVpv| is around zero at MPP. Accordingly, for guaranteeing the intermingling, the VSS-INC must fulfill the accompanying conditon.

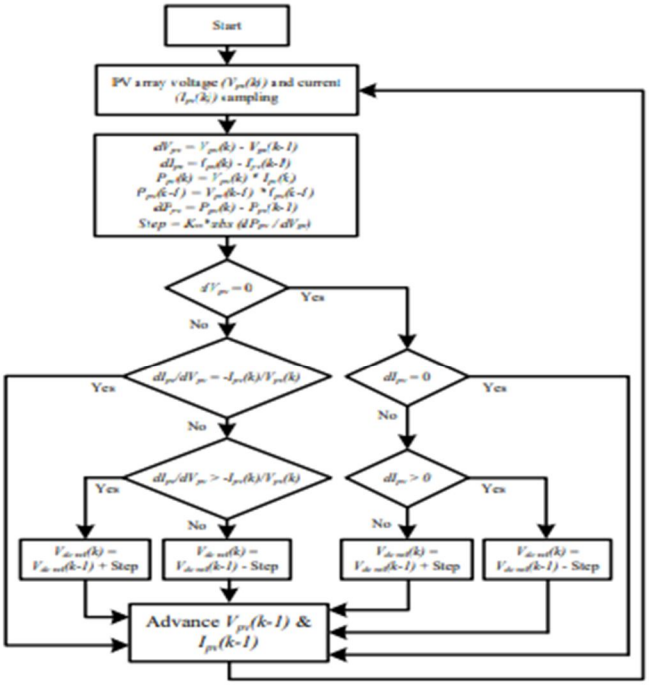

Fig. 3 Single stage VSS-INC algorithm

$$K_{vs} * \left| dP_{pv} / dV_{pv} \right|_{\text{Constant Step} = Step_{max}} < Step_{max}$$

.

The value of the step size constant is, therefore,evaluated as,

$$K_{vs} < Step_{max} / \left| dP_{pv} / dV_{pv} \right|_{\text{Constant Step} = Step_{max}}$$

The VSS-INC keeps operating with step size of Stepmax until (17) is not satisfied. Therefore, (17) gives the boundary limit of the step size constant Kvs for VSS-INC.

III. MODIFIED VECTOR CONTROL

The MVC is sub-divided into two parts. First part is estimation of electromagnetic torque and second part is generation of reference currents and switching signals. The control diagram for SWP pumping using MVC is shown in Fig. 4.

A. Estimation Of Electromagnetic Torque

The estimation of electromagnetic torque (Te est) is carried out in stationary reference frame. V_a, V_b and V_c are obtained from V_{dc} as,

$$V_a = \frac{V_{dc}}{3}(2S_1 - S_3 - S_5)$$

$$V_b = \frac{V_{dc}}{3}(2S_3 - S_1 - S_5)$$

$$V_c = \frac{V_{dc}}{3}(2S_5 - S_1 - S_3)$$

Where, S_1, S_2 and S_5 are the VSI switching signals.

Three phase voltages and currents are converted to stationary voltages (Vα, Vβ) and currents (iα, iβ) using Clark's transformation given as,)

$$V_\alpha = \frac{1}{3}(2V_a - V_b - V_c) \qquad V_\beta = \sqrt{3}(V_b - V_c)$$

$$i_\alpha = \frac{1}{3}(2i_a - i_b - i_c) \qquad i_\alpha = \sqrt{3}(i_b - i_c)$$

The α and β axis stationary flux components (ψ_a and $\psi_ß$) are given as,

$$\psi_\alpha = \int (V_\alpha - R_s i_\alpha)\, dt + \psi_{\alpha 0}$$

$$\psi_\beta = \int (V_\beta - R_s i_\beta)\, dt + \psi_{\beta 0}$$

Where, R_s is the stator resistance, $\psi_{\alpha 0}$ and $\psi_{\beta 0}$ are the initial stationary flux components.

Te $_{est}$ is calculated as,

$$T_{e\,est} = \frac{3}{2} p\,(\psi_\alpha i_\beta - \psi_\beta i_\alpha)$$

Where, p is the number of pole pairs.

B. Generation of Reference Currents and Switching Signals

$V_{dc\ ref}$ generated from VSS-INC method, is compared with V_{dc}. The error at kth sample instant is given as,

$$V_{dc\ error}(k) = V_{dc\ ref}(k) - V_{dc}(k)$$

This error is fed to the DC link PI voltage controller. The DC link voltage controller reduces the error and its output is considered as $\omega r_{ef\,1}$. $\omega_{ref\,1}$ is estimated as,

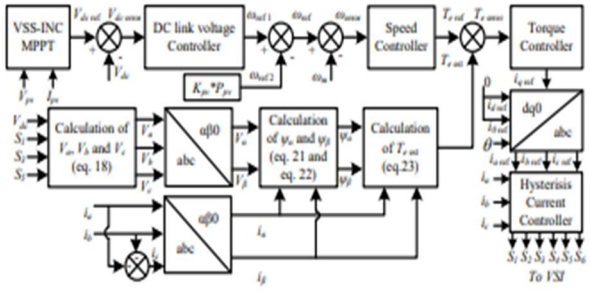

Fig. 4 Control diagram for SWP system

$$\omega_{ref\,1}(k) = \omega_{ref\,1}(k-1) + K_{pd}\{V_{dc\ error}(k) - V_{dc\ error}(k-1)\} + K_{id}V_{dc\ error}(k) \quad (25)$$

Where, K_{pd} and K_{id} are proportional and integral constants, respectively used in DC link voltage PI controller. $\omega_{ref\,2}$ is generated from SPV-FFT such that,

$$\omega_{ref\,2} = K_{pv} * P_{pv} \quad 26$$

Where, K_{pv} is SPV-FFT constant. The maximum value of Kpv can be taken as the ratio of rated power and rated speed, however, the value of K_{pv} is selected from the view point of maximum stability. The reference motor speed ωref is the sum of $\omega_{ref\,1}$ and $\omega_{ref\,2}$.

$$\omega_{ref} = \omega_{ref\,1} + \omega_{ref\,2} \quad 27$$

ωr_{ef} is compared with ω_m and the error at k_{th} sample instant is given as,

$$\omega_{error}(k) = \omega_{ref}(k) - \omega_m(k) \quad 28$$

This error is fed to the speed PI controller. The output of the torque controller is considered as $i_{q\,ref}$ and is given as ,

$$T_{e\,ref}(k) = T_{e\,ref}(k-1) + K_{pa}\{\omega_{error}(k) - \omega_{error}(k-1)\} + K_{ia}\omega_{error}(k) \quad (29)$$

Where, K_{pT} and K_{iT} are proportional and integral constants, respectively used in the torque PI controller.

Thusly, the intelligence level ref is created. For water pumping activity, the engine is worked underneath evaluated speed. Since the speed of the engine is to be controlled below the base speed, no field debilitating activity is required. Accordingly, reference direct axis current ($i_{d\,ref}$) is kept zero. This additionally guarantees solidarity power factor activity. After age of level of $i_{q\,ref}$ and $i_{d\,ref}$, dq0 to abc change is utilized to produce the reference flows ($i_{a\,ref}$, $i_{b\,ref}$ and $i_{c\,ref}$). These reference flows are contrasted and the detected engine flows (ia, ib and ic) and a hysteresis current regulator is utilized for the generation of switching signals.

IV. SYSTEM SIMULATED PERFORMANCE

The performance of this system is investigated through simulation studies. The complete system is simulated using MATLAB/Simulink and its performance is studied during starting and steady state at different insolation levels. The system performance is also studied under dynamic condition. Dynamic response is analyzed through sudden change in insolation and temperature.

The performance is analyzed by assessing the variation in SPV array parameters: insolation (S), SPV array voltage (V_{pv}), SPV array current (I_{pv}) and SPV array power (P_{pv}); PMSM parameters: motor current (i_{abc}), motor speed (ω_m), load torque (T_l) and load power (P_l); and reference parameters: reference DC link voltage (V_{ref}) and reference motor current (i_{ref}).

A. Starting And Steady State Performances

Fig. 5 (a-b) and Fig. 5 (c-d) are illustrating the starting and steady state performance of the system at a solar insolation of 1000 W/m² and 500 W/m² , respectively at a constant temperature of 25 °C. Fig. 5 (a) and Fig. 5 (c) are showing the variation of SPV array parameters, whereas, Fig. 5 (b) and Fig. 5 (d) are showing the variation of PMSM parameters. Fig. 5 (a) and Fig. 5 (c) show that the SPV array voltage (V_{pv}) is effectively following the reference DC link voltage (v_{ref}) obtained from VSS-INC. The SPV array parameters show a very fast convergence. In both the cases, the SPV array parameters are settling within 0.01 s. It is evident from Fig. 5 (b) and Fig. 5 (d) that this control gives a very fast speed response.

The PMSM stator current (i_{abc}) is following the reference current (i_{ref}) obtained using MVC. The motor is drawing twice the steady state current during starting.

Since PMSM is an electromechanical device and has a larger time constant compared to electrical system, the motor parameters are taking more time to come to steady state compared to SPV array parameters. The motor is starting from zero speed and reaching the steady state.

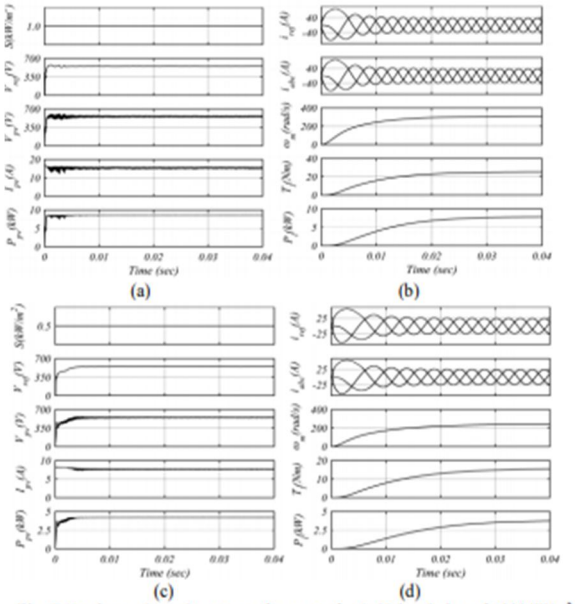

Fig. 5 Starting and steady state performance for (a-b) insolation of 1000 W/m^2 (c-d) insolation of 500 W/m^2

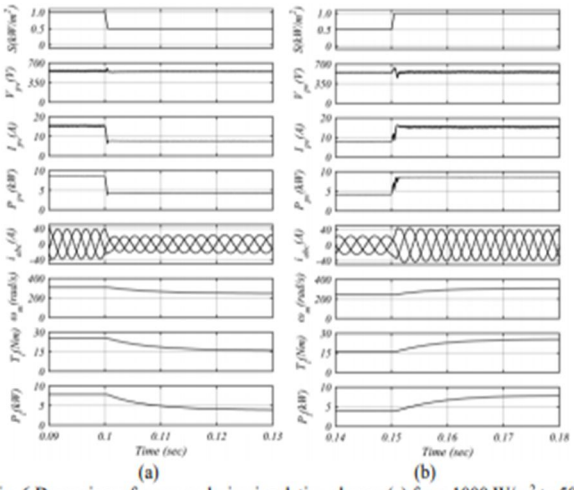

Fig. 6 Dynamic performance during insolation change (a) from 1000 W/m^2 to 500 W/m^2 and (b) from 500 W/m^2 to 1000 W/m^2

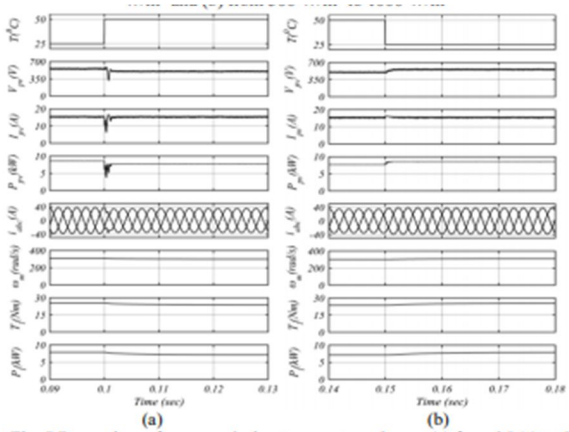

Fig. 7 Dynamic performance during temperature change (a) from 25 °C to 50 °C and (b) from 50 °C to 25 °C

B. Dynamic Performance Under Varying Insolation

Fig. 6 (a) and Fig. 6 (b) are showing the framework dynamic execution during insolation change from 1000 W/m² and 500 W/m² furthermore, from 500 W/m² and 1000 W/m² , separately, at a consistent temperature of 25 °C. Fig. 6 (a) is showing a change in insolation from 1000 W/m² and 500 W/m² at 0.1 s. The insolation change is possibly influencing the SPV cluster voltage (V_{pv}), notwithstanding, enormously influencing the SPV exhibit current (I_{pv}). Since the number of free electrons produced through the breaking of covalent bond because of striking of photons at the PN intersection is relative to sun oriented insolation, the SPV current (I_{pv}) is diminished to practically half for change in insolation from 1000 W/m² and 500 W/m² This is decreasing the SPV capacity to practically a large portion of the appraised esteem. The engine boundaries are likewise differing in like manner. The decrease in insolation is lessening the engine speed (ω_m) and load force (T_l) what's more, at last the heap power (P_l). The framework is settling at another consistent state an incentive for insolation change inside 0.03 s. For the change in insolation from 500 W/m² and 1000 W/m², the framework is performing the other way around.

C. Dynamic Performance Under Varying Temperature

Fig. 7 (a) and Fig. 7 (b) are showing the framework dynamic execution for temperature variety from 25 °C to 50 °C and from 50 °C to 25 °C, individually, at a consistent insolation of 1000 W/m² . Since SPV cluster has a little sure temperature coefficient of current and moderately huge negative temperature coefficient of voltage, the adjustment of temperature is expanding the SPV cluster current (I_{pv}) somewhat yet diminishing the SPV exhibit voltage (V_{pv}) generously. This is bringing about decrease of SPV exhibit power (P_{pv}). The engine speed (ω_m), load force (T_l) and burden power (P_l) are also reducing accordingly and reaching steady state value within 0.03 s. The system performs vice versa when the temperature is restored from 50 °C to 25 °C.

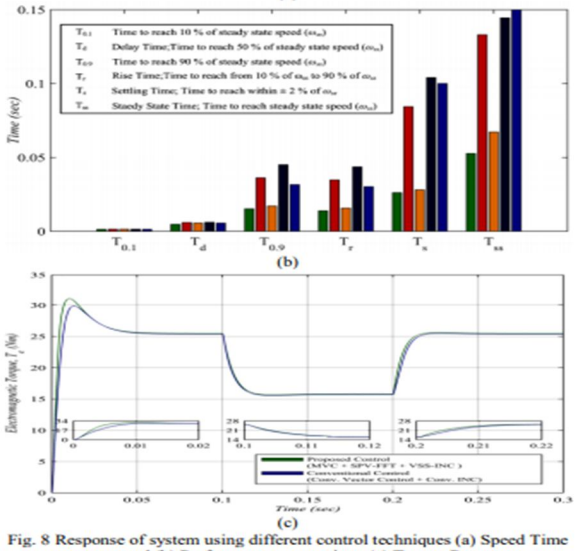

Fig. 8 Response of system using different control techniques (a) Speed Time response and (b) Performance comparison (c) Torque Response

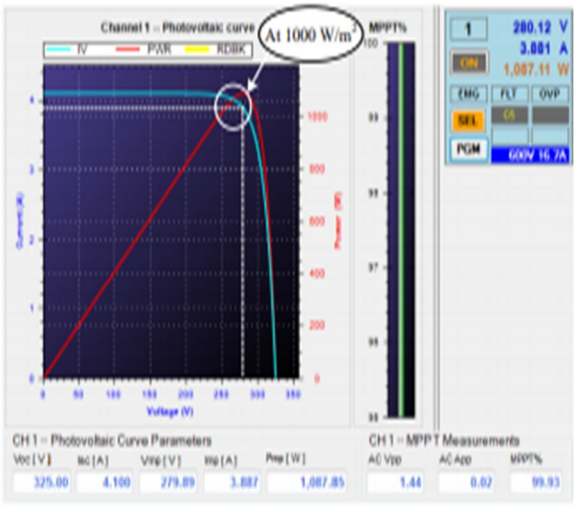

Fig. 9 MPPT performance at STC

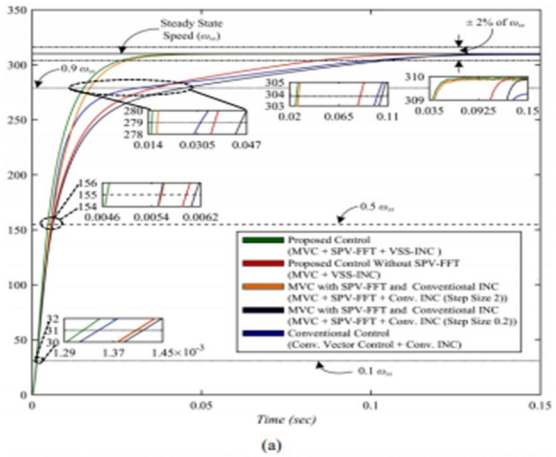

ISSN: 2321-9653; IC Value: 45.98; SJ Impact Factor: 7.429
Volume 9 Issue VII July 2021- Available at www.ijraset.com

D. Comparative Analysis Of Proposed Control With Conventional Control

Fig. 8 (a) presents the speed time reaction of the SWP framework utilizing distinctive control procedures. The near examination is completed at STC. The framework execution is inspected utilizing standard execution measure and the outcomes are illustrated through reference diagram displayed in Fig. 8 (b). Fig. 8 (c) shows the force reaction utilizing proposed and traditional control procedures during beginning, consistent state and keeping in mind that insolation changes from 1000 W/m² and 500 W/m² also, back to 1000 W/m² . Following ends are drawn by contemplating the outcomes displayed in Fig. 8.

1) The conventional control utilizing regular INC MPPT calculation and conventional vector control, gives the sluggish reaction compared with proposed control.

2) The presentation of SPV-FFT speeds up the framework reaction. Without FFT term, the reaction of proposed control turns out to be generally sluggish.

3) Regular INC calculation has an inborn issue for the choice of step size. It is clear from the speed reaction portrayed in Fig. 8 (a) that bigger advance size (2) brings about a consistent state motions in PMSM speed, though, more modest advance size (0.2) displays a drowsy speed reaction and, consequently the framework takes more than 0.15 s to reach ω_{ss}. On the off chance that the progression size is expanded, the motions in speed are expanded, which may destabilize the framework. For a lessening in sync size, the framework sets aside bigger effort to arrive at the consistent state bringing about a lot of force misfortune during dynamic condition.

4) The MVC improves the torque reaction as displayed in Fig. 8. (c). The framework shows a quicker force reaction under all conditions.

5) The proposed control gives the best exhibition among all. The framework displays a quick powerful reaction and zero consistent state speed oscillation.

V. SYSTEM HARDWARE VALIDATION

This system studied in simulation is validated on the experimental laboratory prototype. The experimental prototype comprises of a SPV array simulator (AMETEK make ETS600×17DPVF), a 3 phase VSI (SEMIKRON make MD B6CI 600/415-35F), a PMSM (Motor Power Company make TETRA 115SR5.2) coupled with a DC generator (BENN make) and a resistive load bank. The water pump is realized using a DC generator feeding the resistive load bank. A digital signal processor (DSP–dSPACE1104) is used for controlling the system. A four channel DSO (Agilent make 7014A) with a bandwidth of 100 MHz and a single phase power analyzer (Fluke make 43B) are used for recording test results. Hall-Effect current sensor (LEM make LA55P) and voltage sensor (LEM make LV25P), are used for current and voltage sensing. The DSP gives the output signal in a voltage range of 0-5 V whereas the inverter gate driver circuit requires a 15 V signal for switching of insulated-gate bipolar transistor (IGBT). A NPN BJT (2N2222) based amplifier circuit is used in to provide the necessary amplification from 5 V to 15 V. An opto-coupler (6N136) is used to provide an isolation between the DSP and an inverter gate driver so that any fault onthe inverter side would not affect the DSP. The detailed specifications of PMSM and SPV array used for hardware validation, are given in Appendices. The experimental performance of this system is discussed in the following sections.

A. Performance of SPV Array

The performance of this system is validated for the insolation change from 500 W/m^2 to 1000W/m^2 and temperature variation of 25 °C to 50 °C. The performance of SPV array at STC is shown in Fig. 9. The P_{pv}–V_{pv} curve and I_{pv}–V_{pv} curve are showing an excellent MPP tracking. At STC, the tracking efficiency for modified INC, is found to be 99.93 %.

B. Starting And Steady State Performance

Fig. 10 (a-b) and Fig. 10 (c-d) show the starting performance of this system at 1000 W/m^2 and 500 W/m^2 at 25 °C, respectively. The system is showing a fast starting response. All the system parameters are reaching steady state value as the MPPT algorithm is moving toward the operating point. V_{pv} is coming down from V_{oc} to V_{mpp} as the motor is moving from zero to steady state speed. The motor is attaining a steady state speed of 157 rad/sec at 1000 W/m^{2}and a steady state speed of 95 rad/sec at 500 W/m^2. The rotor position varies from 0 to 2π radian in each rotation. The steady state performances at 1000 W/m2 and 500 W/m2at 25 °Care shown in Figs. 11 (a–b) and Figs. 11 (c–d), respectively. The motor is drawing a sinusoidal current (isa) with a THD less than 5 % under both the conditions as shown in Fig 12 (a) and Fig 12 (b). The values attained by system parameters during steady state at 1000 W/m^2 and 500 W/m^2 are shown in Table I.

C. Performance During Insolation And Temperature Change

The dynamic performance of the system is analyzed by varying the insolation and temperature.

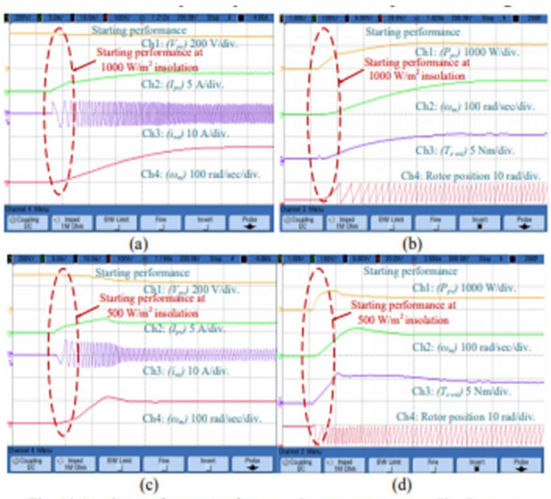

Fig. 10 Starting performance of proposed system parameters V_{pv}, I_{pv}, i_{sa}, ω_m, P_{pv}, $T_{e\,est}$ and Rotor position at (a-b) 1000 W/m² and (c-d) 500 W/m²

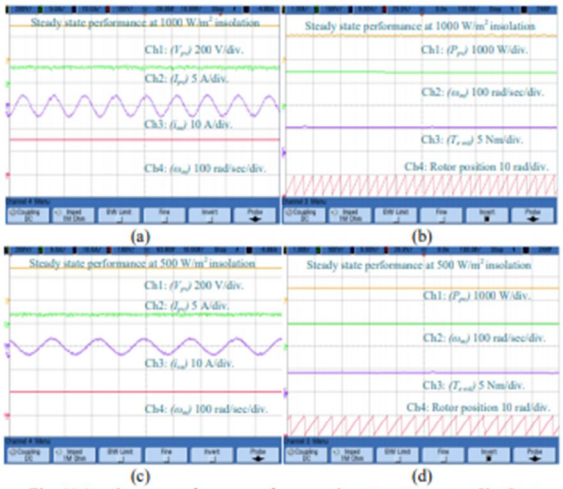

Fig. 11 Steady state performance of proposed system parameters V_{pv}, I_{pv}, i_{sa}, ω_m, P_{pv}, $T_{e\,est}$ and Rotor position at (a-b) 1000 W/m² and (c-d) 500 W/m²

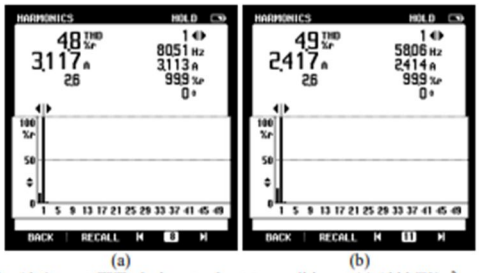

Fig. 12 Current THD during steady state condition at (a) 1000 W/m² and (b) 500 W/m²

Fig. 13 (a) and Fig. 13 (b) are showing the variation of system parameters with an insolation change from 1000 W/m^2 and 500 W/m^2 and from 500 W/m^2 and 1000 W/m^2 , respectively at 25 °C. It can be realized from the system performance that Ipv is dependent on insolation.

TABLE I
STEADY STATE PERFORMANCE OF PROPOSED SYSTEM

Quantity	At 1000 W/m^2	At 500 W/m2
SPV Array Voltage, V_{pv}	280.12 V	272.92 V
SPV Array Current, I_{pv}	3.881 A	1.977 A
Motor phase current, i_{sa}	3.117 A	2.417 A
Speed, ω_m	157 rad/sec	95 rad/sec
SPV Array Power, P_{pv}	1087.11 W	539.56 W
MPPT %	99.93 %	99.2 %
Torque, $T_{e\,est.}$	5.2 Nm	4.2 Nm
Current THD, I_{THD}	4.8 %	4.9 %
MPP Power, P_{mpp}	1087.85 W	543.92 W
Open Circuit Voltage, V_{oc}	325 V	315.22 V
MPP Voltage, V_{mpp}	279.89 V	271.46 V
Short Circuit Current, I_{sc}	4.1 A	2.114 A
MPP Current, I_{mpp}	3.887 A	2.004 A

The temperature change of 25 °C to 50 °C and 50 °C to 25 °C at 1000 W/m2 , are shown Fig. 14 (a) and Fig. 14 (b), separately. It tends to be acknowledged from the procured results that the adjustment of temperature is changing the Vpv. Nonetheless, it isn't influencing Ipv. Vpv is decreasing with an expa**n**sion in temperature and expanding for an abatement in the temperature. As Ipv is staying steady, the adjustment of Vpv is shifting the Ppv and influencing the engine speed in like manner. The engine speed is diminishing for an increment in temperature and the other way around.

VI. CONCLUSION

A SPV array fed SWP system using VSS-INC method for MPPT and MVC for speed control of PMSM, is implemented and performance has been analyzed through MATLAB simulation. Simulation results for starting, steady state and dynamic performances have been found to be quite satisfactory. With the use of VSS-INC technique ,neither the steady state nor the transient performance is compromised as in conventional INC. The MVC has improved the torque response. The introduction of feed-forward term has accelerated the overall response of the system. No steady state oscillations are observed and faster response has made the systemmore effective. Detailed comparative analysis has proven thesuperiority of this control over existing conventional control. The use of PMSM for driving the pump, has increased the systemefficiency and has reduced the system size. The use of single stage topology has eliminated intermediate stage DC-DC converter and reduced the number of components, consequently resulting in reduction of cost, complexity and further increase in the systemefficiency and compactness. Simulation results have found to be quite acceptable and thereby validated the practical feasibility of the system.

VII. FUTURE SCOPE

The work in this thesis is limited to PI controller. With others, the Adaptive Neuro Fuzzy inference system (ANFIS), sliding mode controllers, optimization techniques like genetic algorithm(GA),particle swam optimization(PSO), artificial bee colony algorithm(ABC) etc controllers are used for tuning of PI controller.

VIII. ACKNOWLEDGEMENT

The authors are thankful to Govt. of India, for funding JC Bose project (RP03128) and DST UAY project (RP03222) for financially supporting this work.

A. *Appendices*

1) *PMSM Parameters (Simulation Data):* Stator winding resistance (R_{ss}), 0.11 Ω/ph.; Armature winding inductance (L_s), 97 mH; Torque constant (K_τ), 0.9494 Nm/Arms; Voltage constant (K_v), 57.4 V_{rms}/K_{rpm}; Rated Speed (Nr) 3000 rpm; No. of phases (ph), 3; No. of pole pairs (p), 4; Inertia (I), 0.0016 kg.m^2.
2) *SPV Array Parameters(Experimental Data):* SPV Array Open Circuit Voltage V_{oc}, 325 V; SPV Array MPP Voltage V_{mpp}, 279.89 V; SPV Array Short circuit current I_{sc}, 4.1 A; SPV Array MPP Current I_{mpp}, 3.887 A; SPV Array Maximum Power P_{mpp}, 1087.85 W .
3) *PMSM Parameters (Experimental Data):* Stator winding resistance (R_{ss}), 3.57 Ω/ph.; Armature winding inductance (L_s), 18.33 mH; Torque constant (K_τ), 1.6 Nm/Arms; Voltage constant (K_v), 96.7 Vrms/Krpm; Rated Speed (ω_r) 1500 rpm; No. of phases (ph), 3; No. of pole pairs (p), 3; Inertia (I), 0.00106 kg.m^2.

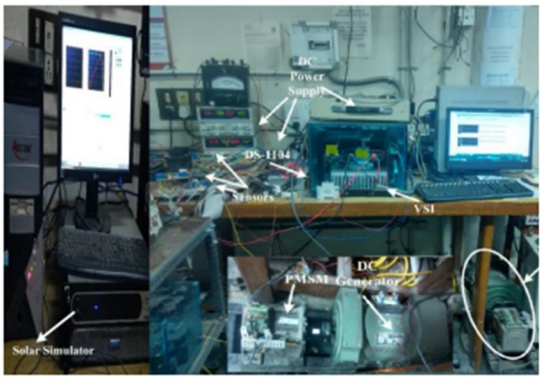

Fig. 15. Photograph of the experimental prototype

REFERENCES

[1] E. T. Maddalena, C. G. d. S. Moraes, G. Bragança, L. G. Junior, R. B. Godoy and J. O. P. Pinto, "A Battery-Less Photovoltaic Water-Pumping System With Low Decoupling Capacitance," IEEE Trans. Ind. Appl., vol. 55, no. 3, pp. 2263-2271, May-June 2019.
[2] R. Kumar and B. Singh, "Grid Interactive Solar PV-Based Water Pumping Using BLDC Motor Drive," IEEE Trans. Ind. Appl., vol. 55, no. 5, pp. 5153- 5165, Sept.-Oct. 2019.
[3] A. Upadhyay, "India rooftop solar power tariff drop to record lows," Livemint, Aug. 29, 2018. [Online]. Available: https://www.livemint.com/Industry/cYZ78fnbiNFt1ppRtRm3JP/India-rooft op-solar-power-tariff-drop-to-record-lows.html [Accessed Nov. 20, 2019].
[4] M. N. Ibrahim, H. Rezk, M. Al-Dhaifallah and P. Sergeant, "Solar Array Fed Synchronous Reluctance Motor Driven Water Pump: An Improved Performance Under Partial Shading Conditions," IEEE Access, vol. 7, pp. 77100-77115, 2019.
[5] M. Rezkallah, A. Chandra, M. Tremblay and H. Ibrahim, "Experimental Implementation of an APC With Enhanced MPPT for Standalone Solar Photovoltaic Based Water Pumping Station," IEEE Trans. Sust. Energy, vol. 10, no. 1, pp. 181-191, Jan. 2019.
[6] S. Murshid and B. Singh, "A Novel Control Scheme for Solar PV Fed PMSM Driven Energy Efficient Water Pumping System," in Proc. 8th IEEE India Int. Conf. on Pow. Elect. (IICPE), Jaipur, India, pp. 1-6, 2018.
[7] R. Syed, M. Mohammad, A. Iqbal, M. Tariq, A. I. Maswood, L. Ben-Brahim and R. A. Al-ammari , "Design and Implementation of Cascaded Multilevel qZSI Powered Single Phase Induction Motor for Isolated Grid Water Pump Application," IEEE Trans. Ind. Appl. [Early Access] DOI: 10.1109/TIA.2019.2959734
[8] J. Meyer and S. V. Solms, "Solar Powered Water Security: An Enabler for Rural Development in Limpopo South Africa," IEEE Access, vol. 6, pp. 20694-20703, 2018.
[9] T. D. Short and M. A. Mueller, "Solar powered water pumps: problems, pitfalls and potential," in Proc. Int. Conf. Pow. Elect., Machines and Drives, (Conf. Publ. No. 487), pp. 280-285, 2002.
[10] S. Murshid and B. Singh, "Implementation of PMSM Drive for a Solar Water Pumping System," IEEE Trans. Ind. Appl., vol. 55, no. 5, pp. 4956-4964, Sept.-Oct. 2019.
[11] R. Antonello, M. Carraro, A. Costabeber, F. Tinazzi and M. Zigliotto, "Energy-Efficient Autonomous Solar Water-Pumping System for Permanent-Magnet Synchronous Motors," IEEE Trans. Ind. Elect., vol. 64, no. 1, pp. 43-51, Jan. 2017.
[12] T. R. Brinner, R. H. McCoy and T. Kopecky, "Induction Versus PermanentMagnet Motors for Electric Submersible Pump Field and Laboratory Comparisons," IEEE Trans. Ind. Appl., vol. 50, no. 1, pp. 174-181, Jan.-Feb. 2014.
[13] B. M. Wilamowski, J. D. Irwin, "Power Electronics and Motor Drives," 2 nd Ed., Boca Raton, Florida, FL, USA, CRC Press, 2017.
[14] F. Niu, K. Li and Y. Wang, "Direct Torque Control for Permanent-Magnet Synchronous Machines Based on Duty Ratio Modulation," IEEE Trans. Ind. Elect., vol. 62, no. 10, pp. 6160-6170, Oct. 2015.
[15] M. H. Vafaie, B. Mirzaeian Dehkordi, P. Moallem and A. Kiyoumarsi, "Minimizing Torque and Flux Ripples and Improving Dynamic Response of PMSM Using a Voltage Vector With Optimal Parameters," IEEE Trans. Ind. Elect., vol. 63, no. 6, pp. 3876-3888, June 2016.
[16] W. Kim and S. Kim, "A Sensorless V/f Control Technique based on MTPA Operation for PMSMs," in Proc. IEEE Energy Conv. Congress and Expo. (ECCE), Portland, OR, pp. 1716-1721, 2018.
[17] Z. Zhang, H. Guo, Y. Liu, Q. Zhang, P. Zhu and R. Iqbal, "An Improved Sensorless Control Strategy of Ship IPMSM at Full Speed Range," IEEE Access, vol. 7, pp. 178652-178661, 2019.
[18] J. Hang, M. Xia, S. Ding, Y. Li, L. Sun and Q. Wang, "Research on Vector Control Strategy of Surface-Mounted Permanent Magnet Synchronous Machine Drive System With High-Resistance Connection," IEEE Trans. Pow. Elect., vol. 35, no. 2, pp. 2023-2033, Feb. 2020.
[19] C. Gong, Y. Hu, J. Gao, Y. Wang and L. Yan, "An Improved DelaySuppressed Sliding Mode Observer for Sensorless Vector-Controlled PMSM," IEEE Trans. on Ind. Elect. [Early Access] DOI: 10.1109/TIE.2019.2952824
[20] A. K. Podder, N. K. Roy and H. R. Pota, "MPPT methods for solar PV systems: a critical review based on tracking nature," IET Renew. Pow. Gen., vol. 13, no. 10, pp. 1615-1632, 2019.
[21] M. A. Elgendy, B. Zahawi and D. J. Atkinson, "Operating characteristics of the P&O Algorithm at high perturbation frequencies for standalone PV systems," IEEE Trans. Energy. Conv., vol. 30, no. 1, pp. 189-198, March 2015.
[22] B. Singh, A. K. Mishra and R. Kumar, "Solar Powered Water Pumping System Employing Switched Reluctance Motor Drive," IEEE Trans. Ind. Appl., vol. 52, no. 5, pp. 3949-3957, Sept.-Oct. 2016.

[23] M. Pokharel, A. Ghosh and C. N. M. Ho, "Small-Signal Modelling and Design Validation of PV-Controllers With INC-MPPT Using CHIL," IEEE Trans. Energy Conv., vol. 34, no. 1, pp. 361-371, March 2019.
[24] L. Yang and Z. Yunbo, "A Novel Improved Variable Step Size INC MPPT Method for PV Systems," in Proc. Chinese Control And Decision Conf. (CCDC), Nanchang, China, pp. 5070-5073, 2019.
[25] D. Venkatramanan and V. John, "Dynamic Modeling and Analysis of Buck Converter Based Solar PV Charge Controller for Improved MPPT Performance," IEEE Trans. Ind. Appl., vol. 55, no. 6, pp. 6234-6246, Nov.- Dec. 2019.

Shadab Murshid (M'15) was born in Patna, Bihar, India, in 1991. He received his B. E in Electrical Engineering from Aligarh Muslim University, Aligarh, India, in 2013. He joined Electrical Engineering Department, Indian Institute of Technology Delhi, India, for M.Tech in 2013. He has completed his Ph. D degree from Indian Institute of Technology Delhi in 2020. His areas of interest includes electric drives, solar water pumping, wind energy conversion systems, applications of adaptive and intelligent control for renewable power generation and power quality improvement in grid interactive renewable energy systems.

Bhim Singh (SM'99, F'10) was born in Rahamapur, Bijnor (UP), India, in 1956. He has received his B.E. (Electrical) from the University of Roorkee (Now IIT Roorkee), India, in 1977 and his M.Tech. (Power Apparatus & Systems) and Ph.D. from the IIT Delhi, India, in 1979 and 1983, respectively. In 1983, he joined the Department of Electrical Engineering, University of Roorkee, as a Lecturer. He became a Reader there in 1988. In December 1990, he joined the Department of Electrical Engineering, IIT Delhi, India, as an Assistant Professor, where he has become an Associate Professor in 1994 and a Professor in 1997. He has been Head of the Department of Electrical Engineering at IIT Delhi from July 2014 to August 2016 He has been Dean, Academics at IIT Delhi , August 2016 to August 2019. He is JC Bose Fellow of DST, Government of India since December 2015. He is CEA Chair Professor since January 2019. Prof. Singh has guided 83 Ph.D. dissertations, and 167 M.E./M.Tech./M.S.(R) theses. He has been filed 52 patents. He has executed more than eighty sponsored and consultancy projects. His areas of interest include solar PV grid interface systems, microgrids, power quality monitoring and mitigation, solar PV water pumping systems, improved power quality AC-DC converters. Authorized licensed use limited to: Fondren Library Rice University.

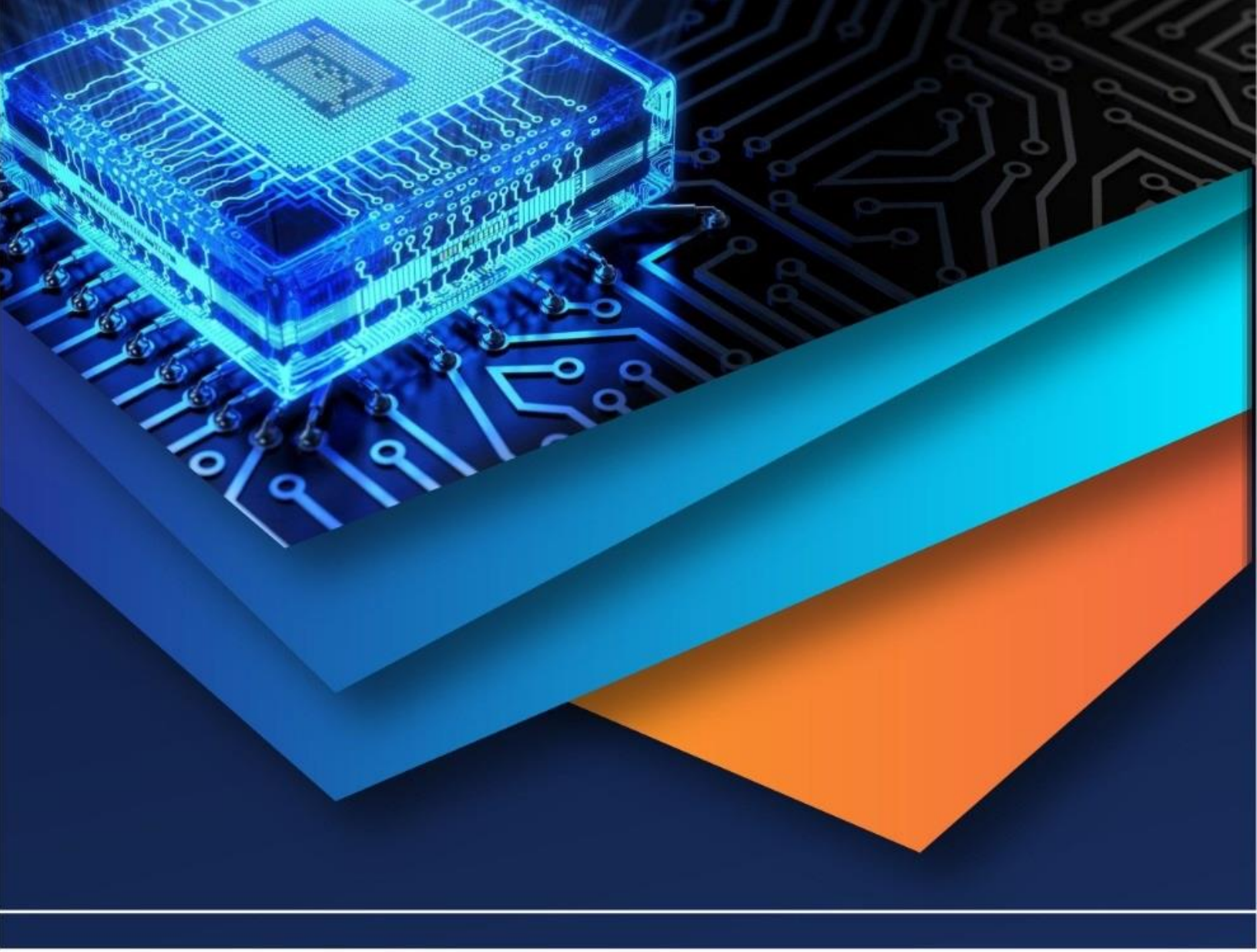

10.22214/IJRASET

45.98

IMPACT FACTOR: 7.129

IMPACT FACTOR: 7.429

INTERNATIONAL JOURNAL FOR RESEARCH

IN APPLIED SCIENCE & ENGINEERING TECHNOLOGY